J Physiol 587.15 (2009) pp 3777–3793

The Journal of Physiology

Claudin-16 affects transcellular Cl^- secretion in MDCK cells

Dorothee Günzel[1], Salah Amasheh[1], Sandra Pfaffenbach[1], Jan F. Richter[1], P. Jaya Kausalya[2], Walter Hunziker[2] and Michael Fromm[1]

[1] *Institute of Clinical Physiology, Charité, Campus Benjamin Franklin, 12200 Berlin, Germany*
[2] *Epithelial Cell Biology Laboratory, Institute of Molecular and Cell Biology, 61 Biopolis Drive, 138673 Singapore, Singapore*

Claudin-16 (paracellin-1) is a tight junction protein localized mainly in the thick ascending limb of Henle's loop and also in the distal nephron. Its defect causes familial hypomagnesaemia with hypercalciuria and nephrocalcinosis. This had been taken as an indication that claudin-16 conveys paracellular Mg^{2+} and Ca^{2+} transport; however, evidence is still conflicting. We studied paracellular ion permeabilties as well as effects of claudin-16 on the driving forces for passive ion movement. MDCK-C7 cells were stably transfected with wild-type (wt) and mutant (R146T, T233R) claudin-16. Results indicated that paracellular permeability to Mg^{2+} but not to Ca^{2+} is increased in cells transfected with wt compared to mutant claudin-16 and control cells. Increased basolateral Mg^{2+} concentration activated a transcellular Cl^- current which was greatly enhanced in cells transfected with wt and T233R claudin-16, as compared to R146T claudin-16-transfected or control cells. This current was triggered by the basolateral calcium-sensing receptor causing Ca^{2+} release from internal stores, thus activating apical Ca^{2+}-sensitive Cl^- channels and basolateral Ca^{2+}-sensitive K^+ channels. Immunohistochemical data suggest that the Cl^- channel involved is bestrophin. We conclude that claudin-16 itself possesses only moderate paracellular Mg^{2+} permeability but governs transcellular Cl^- currents by interaction with apical Ca^{2+}-activated Cl^- channels, presumably bestrophin. As the transepithelial voltage generated by such a current alters the driving force for all ions, this may be the major mechanism to regulate Mg^{2+} and Ca^{2+} absorption in the kidney.

(Resubmitted 2 April 2009; accepted after revision 12 June 2009; first published online 15 June 2009)
Corresponding author D. Günzel: Institut für Klinische Physiologie, Charité Berlin, Campus Benjamin Franklin, Hindenburgdamm 30, 12203 Berlin, Germany. Email: dorothee.guenzel@charite.de

Abbreviations CaSR, calcium sensing receptor; CFTR, cystic fibrosis transmembrane conductance regulator; CLCA, chloride channel, calcium-activated; DCT, distal convoluted tubule; DIDS, 4,4′-diisothiocyanatostilbene-2, 2′-disulphonic acid; DPC, diphenylamine-2-carboxylatem; FHHNC, familial hypomagnesaemia, hypercalciuria and nephrocalcinosis; LLC-PK1 cells, porcine kidney cells; MDCK cells, Madin–Darby canine kidney cells; NMDG, *N*-methyl-D-glucamine; TAL, thick ascending limb of Henle's loop; ZO-1, zonula occludens-1.

The kidneys play a pivotal role in maintaining Mg^{2+} homeostasis of the human body. The main location of Mg^{2+} absorption within the kidney is the thick ascending limb (TAL) of Henle's loop, which accounts for some 70% of Mg^{2+} re-uptake and thus the bulk of the filtrated Mg^{2+}. While the proximal tubule appears to play only a marginal role in Mg^{2+} absorption, the fine-tuning of Mg^{2+} homeostasis takes place in the distal convoluted tubule (DCT; for review see Praga *et al.* 1995; Cole & Quamme, 2000; Meij *et al.* 2002).

Mechanisms of Mg^{2+} absorption differ greatly in the different nephron segments. Mg^{2+} transport in the DCT has been shown to be active transcellular transport, driven by a basolateral Na^+/Mg^{2+} antiport combined with an apical Mg^{2+} influx through Mg^{2+}-permeable channels (such as TRPM6 and 7; for review see Schlingmann & Gudermann, 2005). In contrast, Mg^{2+} transport in the TAL has been demonstrated to be predominantly paracellular, driven by the lumen-positive potential (e.g. Di Stefano *et al.* 1993).

In 1999, Simon *et al.* identified the tight junction protein paracellin-1 which is defective in patients with the rare pathological condition familial hypomagnesaemia with hypercalciuria and nephrocalcinosis (FHHNC, OMIM 248250 and 603959). This protein was found to belong to the claudin family. The paracellin-1 orthologue in cattle was therefore dubbed claudin-16 by Hirano *et al.* (2000) and both terms have since been used synonymously in the literature. Claudins are membrane proteins with four membrane-spanning

DOI: 10.1113/jphysiol.2009.173401

domains and two extracellular loops that are localized in the tight junctions of epithelial and endothelial cells. They interact with intracellular scaffolding proteins of the tight junction complex, such as ZO-1, through a C-terminal PDZ domain binding motif (Itoh *et al.* 1999) and primarily determine paracellular permeability. While many claudins contribute to paracellular barrier formation, at least one, claudin-2, has been shown to form a paracellular channel, rendering specific permeability for small cations to the tight junctions (Amasheh *et al.* 2002). It has therefore been hypothesized that claudin-16 increases paracellular permeability for divalent cations, in particular Mg^{2+} and Ca^{2+}, by forming a paracellular channel, the unusual number of negatively charged amino acids of the first extracellular loop acting as a selectivity filter.

Different forms of claudin-16 exist in rodents and man, designated here as the short and long version. The short version of claudin-16, consisting of 235 amino acids with only 3 intracellular amino acids preceding the first transmembrane region, corresponds to the protein found in mouse and rat and has been suggested to be the physiologically relevant form of claudin-16. The long version is found in man: here, the open reading frame of the claudin-16 mRNA contains two start codons resulting in two proteins that differ in length by 70 amino acids at the cytoplasmic N-terminus (Weber *et al.* 2001*a*). The uncertainty about the two versions led us to study both the short and the long version.

To date, more than 40 mutants of claudin-16 from patients exhibiting FHHNC have been described (Simon *et al.* 1999; Weber *et al.* 2000, 2001*b*; Müller *et al.* 2003, 2006*a*,*b*; for review see Günzel *et al.* 2009*a*). Interestingly, none of the mutations involve the negative charges of the first extracellular loop.

In mouse kidney, claudin-16 is exclusively expressed in the epithelial cells of the TAL (Kiuchi-Saishin *et al.* 2002), which appears to support the hypothesis that claudin-16 forms Mg^{2+}- and Ca^{2+}-permeable channels in this segment of the nephron. However, in rat and human kidney there is evidence for additional expression in the DCT and the collecting duct (rat, Weber *et al.* 2001*a*; human, Simon *et al.* 1999), but in these nephron segments the lumen-negative voltage would not favour but rather counteract paracellular cation absorption. Physiological data are conflicting as well. Ikari *et al.* (2004) report that Ca^{2+} flux in low resistance MDCK cells transfected with claudin-16 cDNA is increased only in the apical-to-basolateral direction. In spite of this increased permeability, claudin-16 expression caused an increase in transepithelial resistance in these cells. Hou *et al.* (2005), on the other hand, found an only slightly enhanced Mg^{2+} permeability without directional preference in low resistance MDCK and LLC-PK1 cells, accompanied by a large increase in Na^+ permeability in the latter cell line. They concluded that the Mg^{2+}-pore hypothesis for claudin-16 is not valid.

In contrast, Kausalya *et al.* (2006) found a moderately increased Mg^{2+} permeability in claudin-16-transfected, high-resistance MDCK-C7 cells compared to mock-transfected controls and cells transfected with various claudin-16 mutants. No changes in the Na^+ *vs* Cl^- permeability ratios were observed and no correlation between Mg^{2+} permeability and transepithelial resistance was detected.

This indicates that – although the effects of claudin-16 mutations on Mg^{2+} loss and Ca^{2+} homeostasis are clinically without doubt – the mechanism of how claudin-16 enhances Mg^{2+} absorption is far from being clear and deserves basic investigation.

In the present study we stably transfected high resistance MDCK cells (MDCK-C7; Gekle *et al.* 1994) (i) with the long or the short version of the functionally intact wild-type (wt) claudin-16, (ii) with the claudin-16 mutant R146T which causes FHHNC phenotype in patients carrying this mutant and which affects the net charge of the second extracellular loop (Weber *et al.* 2001*b*), or (iii) with the claudin-16 mutant T233R which is located in the PDZ-binding motif of claudin-16 and causes a relatively mild form of FHHNC in affected patients (Müller *et al.* 2003). This enabled us to compare the effects of divalent cations on paracellular and transcellular fluxes in claudin-16-transfected cells and mock-transfected control cells.

First, we confirmed and thus corroborated the puzzling fact that claudin-16 only moderately increases paracellular Mg^{2+} permeability. At the same time, basic Ca^{2+} permeability was not significantly altered by claudin-16. However, as a dominating effect, Mg^{2+} and other divalent cations triggered a transcellular Cl^- current by activating the basolateral Ca^{2+}-sensing receptor (CaSR). This current was greatly enhanced in cells transfected with wt claudin-16 compared to control cells and cells transfected with the claudin-16 mutant R146T. In native epithelium, such a current would alter the transepithelial voltage and thus modulate the driving force for the paracellular flux of divalent cations.

Methods

Cell culture and solutions

Monolayers of the high resistance MDCK-C7 cell strain (Gekle *et al.* 1994) were grown in 25 cm^2 culture flasks containing MEM-EARLE (Biochrom, Berlin, Germany), supplemented with 10% (v/v) fetal bovine serum, 100 U ml^{-1} penicillin and 100 mg ml^{-1} streptomycin (Biochrom, Berlin, Germany). Cells were cultured at 37°C in a humidified 5% CO_2 atmosphere.

For electrophysiological measurements and molecular analyses, epithelial cell monolayers were grown on culture plate inserts (pore size 0.45 μm, effective area 0.6 cm^2, Millicell-HA, Millipore, Bedford, MA, USA). Cells were grown to confluence and used on days 6–8 after seeding. Inserts were mounted in Ussing chambers, and water-jacketed gas lifts were filled with 10 ml circulating fluid on each side. The standard bath solution contained: 119 mM NaCl, 21 mM $NaHCO_3$, 5.4 mM KCl, 1.2 mM $CaCl_2$, 3 mM Hepes, and 10 mM D(+)-glucose. The solution was constantly bubbled with 95% O_2 and 5% CO_2, to ensure a pH value of 7.4 at 37°C. To this solution, Mg^{2+} was added as $MgCl_2$ (1 M stock solution, FLUKA, Buchs, Switzerland) or $MgSO_4$ at the desired concentrations (stated for individual experiments). Alternatively, to increase the Mg^{2+} concentration without major changes in osmolarity, appropriate amounts of the standard bath solution were replaced with a bath solution containing 100 mM $MgSO_4$, 19 mM NaCl, 21 mM $NaHCO_3$, 5.4 mM KCl, 1.2 mM $CaCl_2$, 3 mM Hepes, and 10 mM D(+)-glucose.

To obtain Na^+-free bath solutions, NaCl was replaced with equimolar amounts of NMDG-Cl, while $NaHCO_3$ was replaced with equimolar amounts of cholin-HCO_3. In low K^+ bath solutions, KCl was omitted without substitution. In high K^+ bath solutions the desired amount of NaCl was replaced with KCl to maintain osmolarity. Several different Cl^--free solutions were applied: all Cl^- was either replaced with gluconate, with nitrate or with pyruvate. As gluconate binds divalent cations, Ca^{2+} concentrations in gluconate-containing solutions were increased to 10 mM.

Cloning and transfection procedures

Molecular cloning of claudin-16 cDNA was performed by PCR with respective sense (5′-CTTCGGATAATGACCTCCAGG-3′) and antisense (5′-ACGTGCATTTTACACCCTTGT-3′) oligonucleotides (Simon *et al.* 1999) using human universal quick clone cDNA as template (Clontech Laboratories Inc., Mountain View, CA, USA). The resulting 936 bp PCR product encompassing the complete claudin-16 cDNA was cloned into pGEMT-Easy (Promega, Madison, WI, USA). Similarly, claudin-11 cDNA was cloned from kidney cDNA (generous gift from Dr Dominik Müller, Charité, Berlin) using sense (5′-ATGGTGGCCACGTGCCTGCAGG-3′) and antisense (5′-CTATACGTGGGCACTCTTCGCATG-3′) oligonucleotides. Claudin-16 mutants R146T and T233R were cloned as recently reported (Kausalya *et al.* 2006). The correctness of the cDNA was verified by sequencing and the mutants, the short ('rodent', 708 bp), and the long version of claudin-16 ('human', 918 bp) and claudin-11 were subcloned into the eukaryotic expression vectors pcDNA3 (Invitrogen, Carlsbad, CA, USA) and pFLAG-CMV4 (Sigma Aldrich, St Louis, MO, USA), respectively. The long version of claudin-16 was also subcloned into a modified pcDNA3.1 vector (generous gift from O. Huber, Charité, Berlin), tagging the N-terminus of claudin-16 with yellow fluorescence protein (YFP). MDCK-C7 cells were stably transfected employing the Lipofectamine plus method (Gibco BRL, Invitrogen Corp., Gaithersburg, MD, USA). G418-resistant cell clones were screened for claudin-16 expression by Western blot analysis and immunohistochemistry. MDCK-C7 cells mock-transfected with respective empty vectors and with claudin-11 served as controls.

PCR

RNA was extracted from claudin-16- and vector-transfected MDCK-C7 cells using the NucleoSpin RNA/protein kit (Macherey-Nagel, Düren, Germany) according to the instructions of the manufacturer. cDNA was synthesized from 4 μg total RNA using the High Capacity cDNA Archive Kit (Applied Biosystems, Foster City, CA, USA) in a 40 μl reaction volume.

PCR for bestrophin-1 to -4 was performed on MDCK-C7 cDNA and on commercial dog kidney cDNA (BioChain, Hayward, CA, USA) using HOTSTAR DNA polymerase (Qiagen, Hilden, Germany) and the following primers: bestrophin-1, forward 5′-GGAGGAAGAGGAAGGCACTC-3′, reverse 5′-AGGCTTGAGGGTGCTGACT-3′, alternative reverse 5′-TGTGGACGGCTGTATGGCTGTGAC-3′; bestrophin-2, forward 5′-GCCAAAGAGGACATGCAGTT-3′, reverse 5′-GCATAGGCACAGTGGTGAAG-3′; bestrophin-3, forward 5′-GGAGGAAGAGGAAGGCACTC-3′, reverse 5′-ACTCGGCTCGACTCCTGTAA-3′; bestrophin-4 forward 5′-AAACCTCGGGAGCCTTTAGA-3′, reverse 5′-CGAAGGTTGAAGGTGGAG-3′. Cycling conditions were: 45 s 95°C, 60 s 60°C and 120 s 72°C for 35 cycles with an initial denaturation of 15 min and final extension of 8 min.

TaqMan real-time PCR was performed using the following probes (Applied Biosystems, Foster City, CA, USA): bestrophin-1, Cf02697409_gH; bestrophin-4, Cf02718712_m1, calcium sensing receptor, Cf02741809_s1, and β-Actin (part number 4310881E) as an endogenous control.

Western blot analysis

Western blot analysis was carried out as described in detail by Amasheh *et al.* (2002). Claudin-16 and claudin-16 mutants were detected by immunoblotting, employing antibodies raised against human claudin-16 (Zymed

Laboratories, Invitrogen Immunodetection, South San Francisco, CA, USA), against the FLAG-tag or against the HA-tag (Sigma Aldrich), as appropriate. Control blots showed no differences for the major MDCK claudins (1–5, 7, 8) between mock-transfected control cells and claudin-16-transfected cells (see online Supplementary Fig. S1).

Immunohistochemistry/laser scanning microscopy

For immunohistochemical studies, cells were grown on transparent culture plate inserts (pore size 0.4 μm, effective area 0.6 cm^2, Millicell-PCF, Millipore). Cells were rinsed with PBS, fixed with methanol, and permeabilized with PBS containing 0.5% Triton X-100. Primary antibodies employed were mouse anti-occludin and rabbit anti-claudin-16 (Zymed Laboratories), and rabbit anti-bestrophin-1, Abcam ab14927 (Abcam, Cambridge, MA, USA). Concentrations of primary antibody were 10 μg ml^{-1}. Secondary antibodies Alexa Fluor 488 goat anti-mouse and Alexa Fluor 594 goat anti-rabbit (both used at concentrations of 2 μg ml^{-1}) were purchased from Molecular Probes (Eugene, OR, USA). DAPI (4′,6-diamidino-2-phenylindole dihydrochloride, 1 μM) was used to stain cell nuclei. Fluorescence images were obtained with a confocal microscope (Zeiss LSM510, Carl Zeiss, Jena, Germany) using excitation wavelengths of 543 nm, 488 nm and 405 nm.

Electrophysiology and flux measurements

Short circuit current (I_{SC}, μA cm^{-2}) was measured in Ussing chambers specially designed for insertion of Millicell filters (Kreusel *et al.* 1991). Resistance of bath solutions and filter support was measured prior to each single experiment and taken into account for I_{SC} data. In all figures, positive I_{SC} values indicate anion secretion (i.e. movement from the basolateral to the apical side) and/or cation absorption (i.e. movement from the apical to the basolateral side). In some experiments, ion gradients were applied across the cell layer, so that, strictly, the term short circuit current does not apply. In these experiments, the current necessary to clamp the transepithelial potential to 0 mV is dubbed 'holding current', I_h. All traces shown in Figs 3–6 are typical examples of at least three independent experiments.

Measurement of unidirectional tracer flux was performed under short circuit conditions with 50 kBq ml^{-1} ^{45}Ca (Amersham Biosciences, Piscataway, NJ, USA). The medium also contained non-labelled tracer molecules (1.2 mM $CaCl_2$). Ten minutes after addition of the tracer, two 100 μl samples were taken from the donor side, and 900 μl standard bathing solution and 4 ml of Ultima Gold high flash-point liquid scintillation cocktail (Packard Bioscience, Groningen, The Netherlands) were added to each sample. Samples (1 ml) of the receiving side, replaced with fresh standard bath solution, were mixed with 4 ml of the liquid scintillation cocktail. All 5 ml samples were subsequently analysed with a Tri-Carb 2100TR Liquid Scintillation counter (Packard, Meriden, CT, USA).

As radioactive Mg isotopes are not readily available, Mg^{2+} flux was measured employing atomic absorption sprectrometry (AAS). Prior to these experiments Ussing chambers were scrupulously cleaned, using a 10 mM EDTA solution, and rinsed several times with bidistilled water.

Cells grown on filter supports were washed twice in nominally Mg^{2+}-free solution, mounted in the Ussing chambers and equilibrated in nominally Mg^{2+}-free bath solutions for 15 min. A 1 ml sample was taken from the appropriate side (basolateral or apical) and the solution was replaced with 1 ml nominally Mg^{2+}-free bath solution before 10 mM Mg^{2+} was added to the other side, by replacing 1 ml Mg^{2+}-free bath solution with 1 ml 100 mM Mg^{2+} bath solution. After the addition of Mg^{2+}, 1 ml samples were taken from the low Mg^{2+} side every 30 min (replaced with 1 ml nominally Mg^{2+}-free solution). Five microlitres of a solution containing 20% La_2O_3 in 32% HCl were added to the samples to minimize anion interference and the Mg^{2+} content was measured with a Perkin-Elmer 2380 atomic absorption spectrometer (Perkin-Elmer, Waltham, MA, USA).

As this method requires the use of a nominally Mg^{2+}-free solution on the acceptor side, dilution potentials were measured as an alternative method to evaluate permeabilities to mono- and divalent cations, as described in detail by Günzel *et al.* 2009*b*.

Microfluorimetric measurements

All microfluorimetric measurements were carried out in nominally HCO_3^--free, Hepes-buffered solutions (composition see above). Filter membranes from culture plate inserts (pore size 0.4 μm, effective area 0.6 cm^2, Millicell-PCF) covered with confluent cell monolayers were carefully cut out and incubated with 10 μM fura-2 AM (Molecular Probes) in Hepes-buffered saline for 30 min at room temperature. Subsequently, filters were mounted in the perfusion chamber (apical side down) attached to an inverted microscope (Zeiss Axiovert 100) and washed for 30 min to remove excess extracellular dye and to allow complete conversion of intracellular fura-2 AM to the free fura-2 acid. Fluorescence was excited with light from a xenon lamp (XPO 75 W/2; Osram, Munich, Germany) filtered by two rotating filters (6 s^{-1}) at 340 and 380 nm. Emitted light was detected at 510 nm by a photomultiplier (928 SF; Hamamatsu, Hamamatsu, Japan) connected to an EPC-9 patch-clamp amplifier. Data were stored and processed on a PC using TIDA

for Windows. Relative changes in $[Ca^{2+}]_i$ are represented by changes in the 340/380 nm fluorescence ratio while absolute $[Ca^{2+}]_i$ was calculated using the equation and dissociation constant of Grynkiewicz *et al.* (1985) as previously described by Hochstrate *et al.* (1995).

Results

After transfection, the proper localization of the long ('human') version of claudin-16 within the tight junction was derived from staining against the FLAG-tag or from the fluorescence signal of the YFP fused to the N-terminus of the claudin-16 (Fig. 1). Localization of the short ('rodent') version has been described in a previous study (Kausalya *et al.* 2006).

Paracellular Mg^{2+} and Ca^{2+} permeability of claudin-16-expressing cell layers

Mg^{2+} permeabilities (P_{Mg}) of MDCK cell layers kept in Ussing chambers (transepithelial potential, V_{epi}, clamped to 0 mV) were investigated using atomic absorption spectrometry, as previously described (Kausalya *et al.* 2006). This technique requires the application of a Mg^{2+} gradient (*cis* 10 mM, *trans* nominally 0 mM). Under these conditions, P_{Mg} was found to be increased in wt claudin-16-expressing cells (long and short version) compared to R146T or T233R claudin-16-expressing cells and control cells (Fig. 2*A*).

Ca^{2+} permeabilities (P_{Ca}) were determined from $^{45}Ca^{2+}$ flux measurements in Ussing chambers (V_{epi} clamped to 0 mV). In contrast to P_{Mg}, P_{Ca} was determined under symmetrical Ca^{2+} conditions (1.2 mM Ca^{2+} on the apical and basolateral side) to avoid disruption of tight junctions at low Ca^{2+} concentrations. Under these conditions, P_{Ca} was approximately 50% of P_{Mg} determined in mock-transfected cells and did not differ significantly between mock-transfected, claudin-16-transfected and R146T mutant-transfected cells (Fig. 2*B*).

As transport kinetics under symmetrical and zero-trans conditions may differ, Ca^{2+}, Mg^{2+} and Na^+ permeabilities were additionally determined by measuring dilution/biionic potentials in control and wt claudin-16-transfected cell layers. As shown in Fig. 2*C*, under these conditions P_{Mg} and P_{Ca} were similar. While control and wt claudin-16-transfected cell layers did not differ in P_{Na} and P_{Ca}, P_{Mg} was significantly increased in wt claudin-16-transfected cell layers.

Increased Mg^{2+}-induced transcellular current in wt claudin-16-transfected MDCK cells

Wt claudin-16-expressing cells differed from controls not only with respect to their paracellular transport properties, but unexpectedly also with respect to a transient, transcellular current elicited by an increase in extracellular Mg^{2+}. This current was concentration dependent (Fig. 3*A*) with a half-maximal response concentration (EC_{50}) of

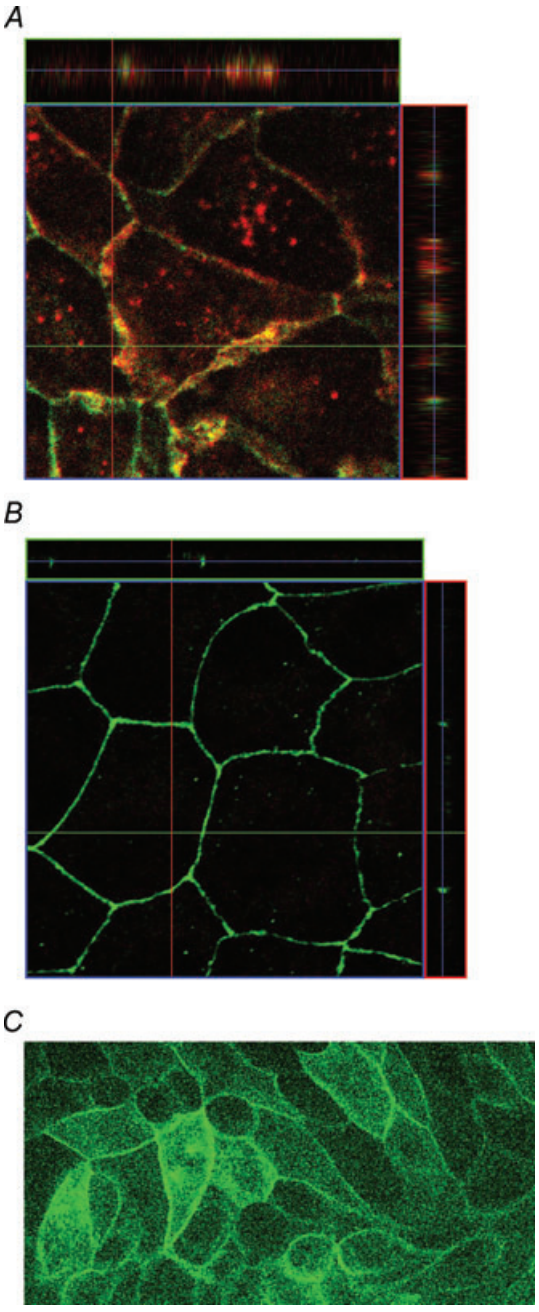

Figure 1. Localization of wt claudin-16 (long version) expressed in MDCK cells
A, immunohistochemical staining indicates co-localization of the long 'human' wt claudin-16 version in cells expressing claudin-16 (red: anti-Flag antibody) with the tight junction marker occludin (green). *B*, mock-transfected control. *C*, also the YFP–claudin-16 fusion protein is localized within the tight junction (green, YFP fluorescence). Localization of the short wt claudin-16 variant and the mutants R146T and T233R has been studied previously (Kausalya *et al.* 2006).

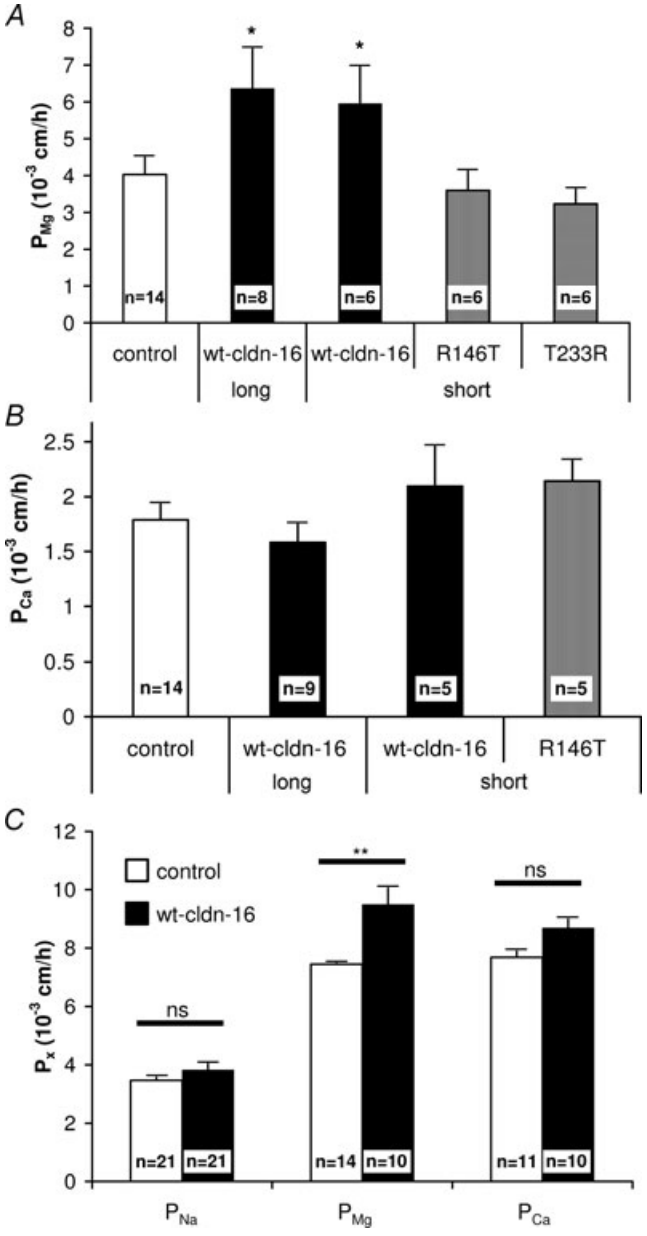

Figure 2. Paracellular Mg^{2+} and Ca^{2+} permeability
A, paracellular Mg^{2+} permeability, calculated from Mg^{2+} flux measurements, was increased ($P < 0.05$, unpaired *t* test) in MDCK-C7 cell layers transfected with either the long or the short version of wt claudin-16 compared to mock-transfected control cells while Mg^{2+} permeability of mutant (R146T, T233R) claudin-16-transfected cell layers was unchanged. *B*, paracellular Ca^{2+} permeability, calculated from $^{45}Ca^{2+}$ flux measurements, did not differ in wt or mutant claudin-16-transfected MDCK-C7 cell-layers compared to mock-transfected control cells. *n*, number of independent experiments. *C*, Na^+, Mg^{2+} and Ca^{2+} permeabilities, calculated from dilution potential/biionic potential measurements on wt claudin-16 (long version) and mock-transfected MDCK-C7 cell layers. Mg^{2+} permeability was increased in claudin-16-transfected compared to mock-transfected cells ($P < 0.01$, unpaired *t* test), while no significant differences were found for Ca^{2+} or Na^+ permeabilities. All values mean ± S.E.M.

5.2 mM and a Hill coefficient of 2.3. The current could be elicited by Mg^{2+} simultaneously applied to both sides of the epithelium or by application to the basolateral side alone, but not by application to the apical side alone, and was thus solely due to Mg^{2+} applied to the basolateral side (Supplementary Fig. S2). The direction of

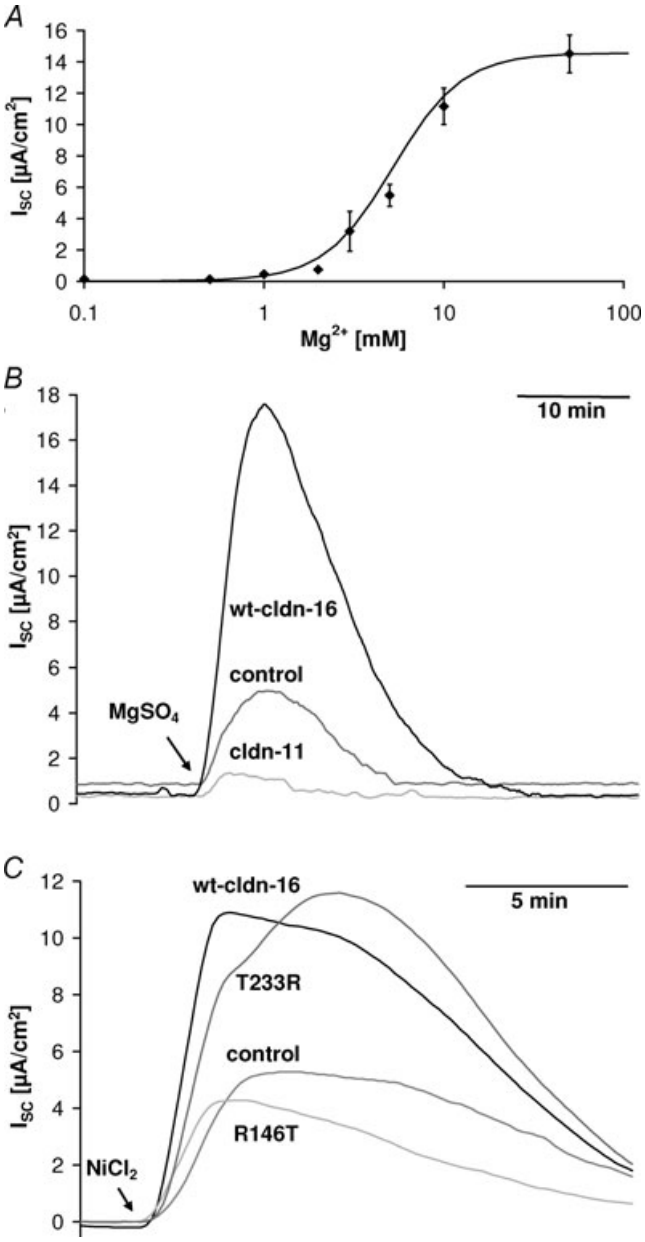

Figure 3. Divalent cation-induced transcellular current
A, dose–response curve for the transcellular current induced by basolateral Mg^{2+} application in wt claudin-16-transfected MDCK cells. EC_{50}, 5.2 mM; Hill coefficient, 2.3. *B* and *C*, application of divalent cations (*B*, 10 mM $MgSO_4$; *C*, 100 μM $NiCl_2$) to the basolateral side induced a transcellular current (short circuit current, I_{SC}) that was considerably larger in wt claudin-16-transfected (*B*, long version; *C*, short version) and T233R mutant-transfected cell layers than in R146T mutant claudin-16-transfected, in mock-transfected control cell layers, and, for comparison in claudin-11-transfected cells.

the current indicated either net anion secretion or net cation absorption. The current was accompanied by a decrease in transepithelial resistance (R_t) and an increase in the transepithelial voltage difference (Supplementary Fig. S3).

The Mg^{2+}-induced current was larger in cells expressing the long or the short version of wt claudin-16 than in mock-transfected control cells or, as a further control, in claudin-11-transfected cells. In cells transfected with the claudin-16 mutant R146T, the current was comparable to the current observed in control cells, while in cells transfected with the claudin-16 mutant T233R the current was similar to that observed in wt claudin-16-transfected cells (Fig. 3*B* and *C*). As cells expressing the long or the short version of wt claudin-16 showed the same properties, no further distinction is made between these two versions and the pooled results are referred to as wt claudin-16-transfected cells. The current was independent of the anion of the Mg^{2+} salts used (e.g. $MgCl_2$ *vs* $MgSO_4$) and could not be elicited by osmotically equivalent amounts of NaCl or mannitol (not shown), ruling out that the current might be induced by cell volume changes.

A transient current with the same properties as the Mg^{2+}-induced current, but with different magnitude, could also be activated by a basolateral application of millimolar concentrations of $CaCl_2$ or the polyamine spermidine, or (as depicted in Fig. 4*A*) by micromolar concentrations of $CdCl_2$, $CoCl_2$, $NiCl_2$, $MnCl_2$, and $ZnCl_2$, but not e.g. by cobalt hexaammine (an analogue of the hydrated Mg^{2+} ion), $CuSO_4$ or $SnCl_2$. Independent of the ion used for activation, the divalent cation-induced current was strongly dependent on the extracellular pH value. It was greatly enhanced at alkaline pH values and reduced at acidic pH values (Fig. 4*B*). Again, the current was larger in cells expressing the long or the short version of wt claudin-16 than in mock-transfected control cells. The current could be activated both in the presence and in the nominal absence of extracellular Mg^{2+}.

The fact that the current could only be stimulated from the basolateral side, the spectrum of activating substances, the EC_{50} and Hill coefficient derived from the dose–response curve and the pH dependence, suggested that the current was due to an activation of the basolateral calcium (and magnesium)-sensing receptor (CaSR, for review see e.g. Chang & Shoback, 2004).

This assumption implies that wt claudin-16 interacts either with CaSR or with one of the processes triggered by CaSR activation. To investigate this hypothesis, this divalent cation-induced current was further characterized. As the relatively high $MgSO_4$ concentrations needed to elicit the current would impair strict short circuit conditions, many of the following experiments were carried out using 100 μM $NiCl_2$.

Na^+ and K^+ dependence of the claudin-16-dependent cation-induced current

The divalent cation-induced current was completely inhibited in nominally Na^+-free solutions (Na^+ replaced with $NMDG^+$). Further experiments demonstrated that it was sufficient to replace Na^+ on the basolateral side, while replacement on the apical side had no effect (Fig. 4*C*).

All changes in the extracellular K^+ concentration (reduction to nominally 0 K^+ and 0.1 mM K^+, increase to 10, 20, 30, 60 or 120 mM K^+) decreased the divalent cation-induced current, irrespective of the direction of the change. As seen with changes in the extracellular Na^+ concentration, variations in the extracellular K^+ concentration were only effective on the basolateral side.

Thus, effects of variations in the extracellular K^+ concentration were difficult to interpret. This was attributed to the fact that changes in the extracellular K^+ concentration cause changes in the membrane potential and thus in the driving force for ion transport. At the highest K^+ concentrations of 60 or 120 mM, the observed inhibition of the divalent cation-induced current might well be due to the concommitant decrease in Na^+. Conversely, using nominally K^+-free solutions on the basolateral side would, in addition, block the Na^+/K^+ pump. Control experiments showed, however, that using up to 0.4 mM ouabain to block the divalent cation-induced current was considerably less potent than the use of nominally K^+-free solutions, so that there appeared to be an absolute requirement for basolateral K^+ (Fig. 4*D*). This conclusion was supported by the finding that furosemide (up to 0.2 mM) also partially blocked the divalent cation-induced current (Fig. 4*E*) and the combined application of bumetanide (0.1 mM) and chlorothiazide (0.1 mM, Fig. 4*F*) caused an almost complete inhibition.

The divalent cation-induced current was also partially blocked by a basolateral application of the Ca^{2+}-activated K^+ channel blocker charybdotoxin (10^{-7} M), and the K^+ channel blockers glibenclamide (0.2 mM) and Ba^{2+} (5 mM). In contrast, neither an apical application of Ba^{2+} nor the application of the maxi-K^+ channel blocker iberiotoxin (10^{-7} M) had any effect (not shown).

HCO_3^-- and Cl^--dependence of the claudin-16-dependent cation-induced current

Using HCO_3^-/CO_2-free solutions (Hepes-buffered and equilibrated with 100% O_2) had no effect on the divalent cation-induced current (not shown).

The dependence of the divalent cation-induced current on Cl^- was investigated by replacing Cl^- with gluconate, pyruvate or nitrate. Gluconate has the disadvantage of binding divalent cations, so that the free Mg^{2+} and Ca^{2+} concentrations in gluconate-based solutions with

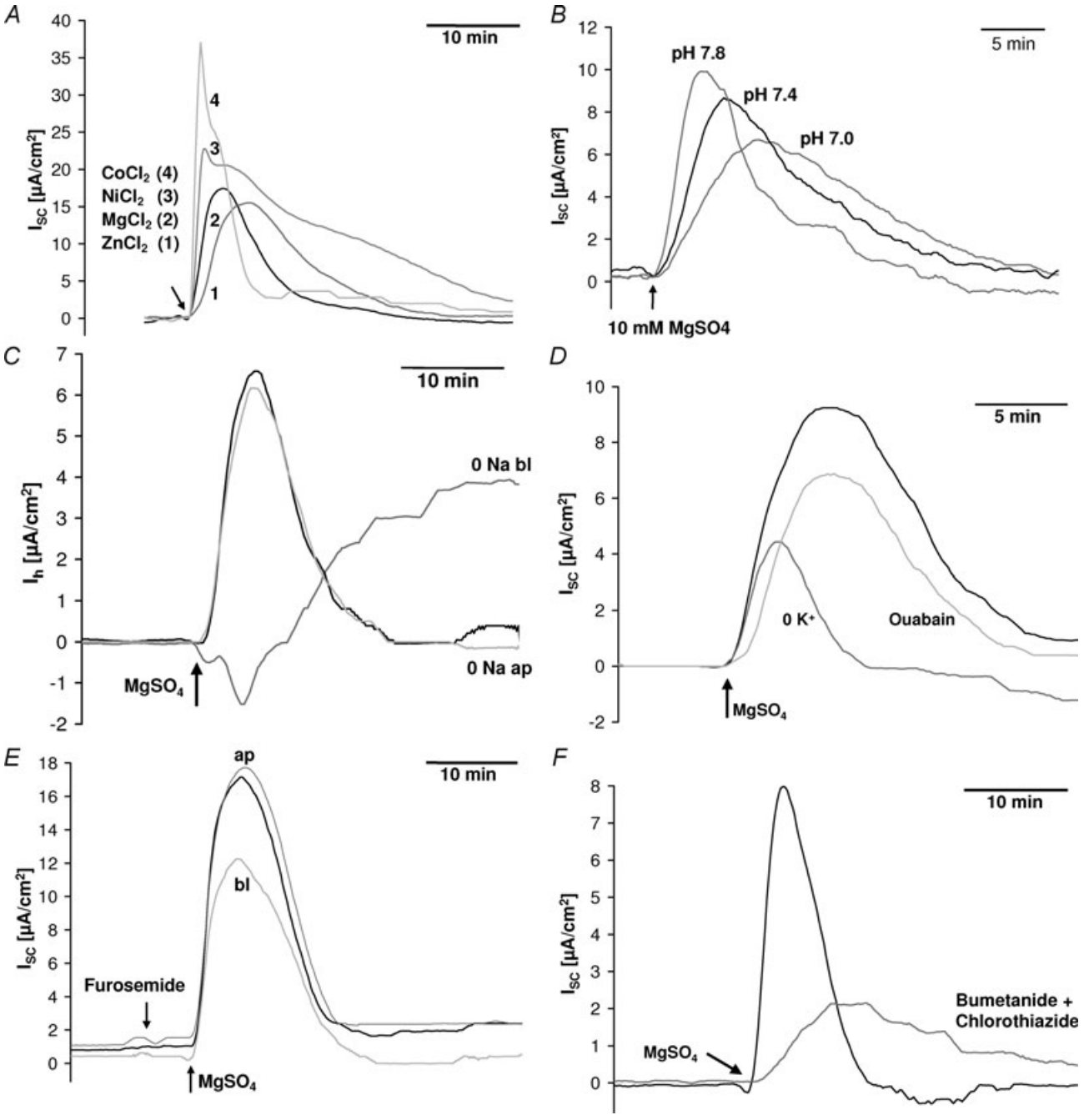

Figure 4. Divalent cation-induced transcellular current: cation contribution
A, comparison of current responses to a basolateral application of 100 μM $ZnCl_2$, 10 mM $MgCl_2$, 100 μM $NiCl_2$ and 100 μM $CoCl_2$, respectively, to wt claudin-16-transfected cell layers. *B*, the current response (elicited by the application of 10 mM $MgSO_4$, short wt claudin-16-transfected cells) was strongly dependent on the extracellular pH. *C*, reduction of Na^+ to nominally 0 mM on the basolateral side inhibited the divalent cation-induced current (10 mM $MgSO_4$). *D*, reduction of K^+ to nominally 0 mM on the basolateral side partially inhibited the divalent cation-induced current (10 mM $MgSO_4$). This was not due to an inhibition of the Na^+/K^+ pump, as preincubation with 400 μM ouabain had only small effects. *E*, the divalent cation-induced current (10 mM $MgSO_4$) was partially blocked by an application of 200 μM furosemide to the basolateral but not to the apical side. *F*, a combined application of 100 μM bumetanide and 100 μM chlorothiazide almost completely blocked the divalent cation-induced current (10 mM $MgSO_4$). I_{SC}, short circuit current. I_h, holding current necessary to clamp the transepithelial potential to 0 mV in the presence of an ion gradient across the cell layer.

unchanged total Mg^{2+} and Ca^{2+} concentrations are lower than in Cl^--based solutions. Nevertheless, the effect of gluconate- and pyruvate-based solutions on the divalent cation-induced current was identical: the current was completely blocked if Cl^- was replaced on the basolateral side, but it was enhanced if Cl^- was replaced on the apical side of the cell layer (Fig. 5*A*). Replacement of Cl^- by nitrate had the opposite effect; it enhanced the

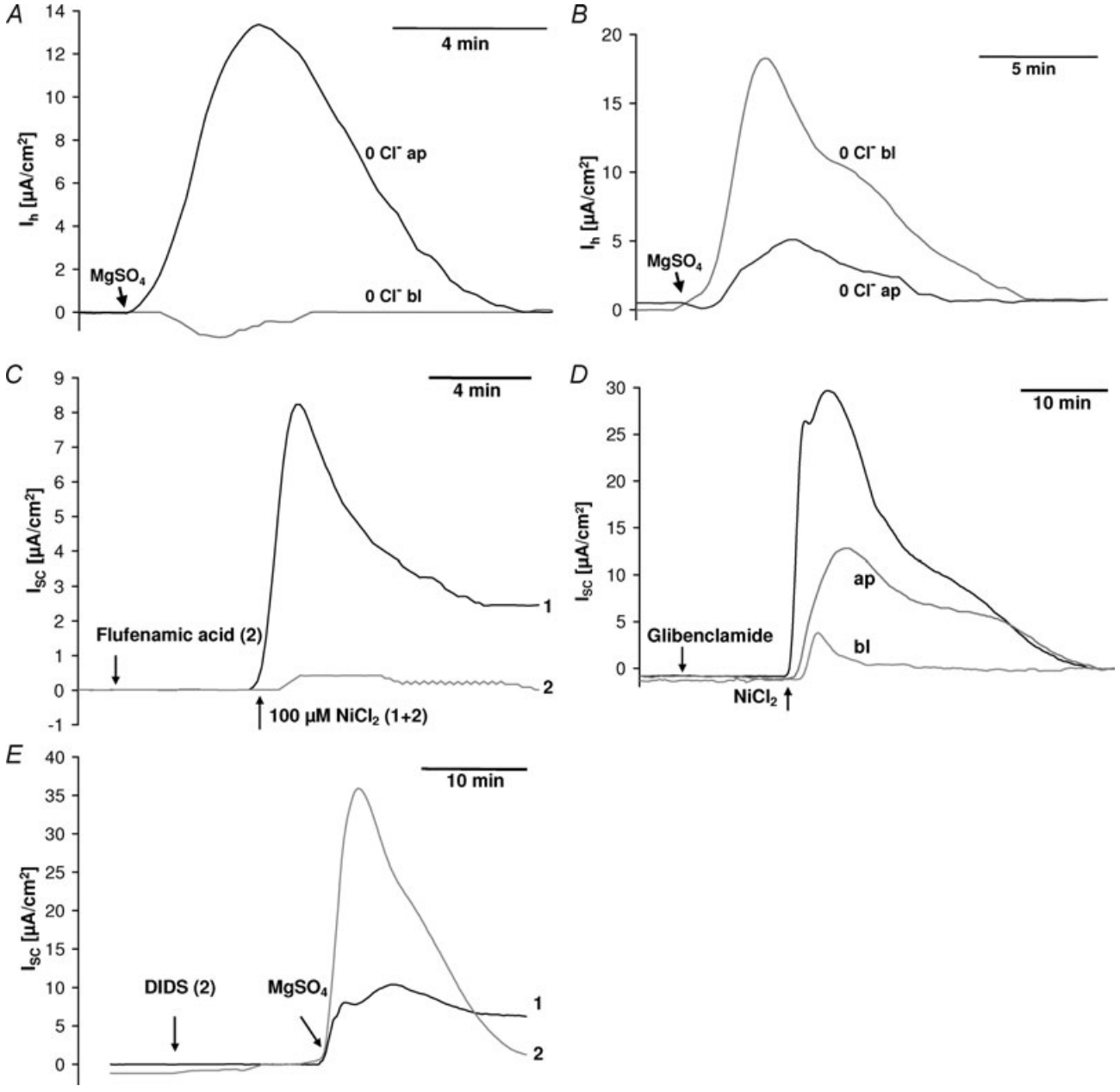

Figure 5. Divalent cation-induced transcellular current: anion contribution
A and *B*, Cl^- was replaced with pyruvate or nitrate, either in the basolateral or the apical side throughout the entire experiment. *A*, the divalent cation-induced current (10 mM $MgSO_4$) was completely blocked if basolateral Cl^- was replaced with pyruvate (or gluconate, not shown), while an apical replacement had no effect or even caused a slight increase in current. *B*, in contrast to *A*, replacing basolateral Cl^- with nitrate increased the divalent cation-induced current (10 mM $MgSO_4$) while an apical replacement greatly reduced the current. *C*, the divalent cation-induced current (100 μM $NiCl_2$) was inhibited by very low concentrations (0.2 μM) of the Cl^- channel blocker flufenamic acid. *D*, the K^+ and CFTR Cl^- channel blocker glibenclamide (0.2 mM) was more effective in blocking the divalent cation-induced current (100 μM $NiCl_2$) when applied to the basolateral than to the apical side of the cell layer. *E*, basolateral application of 100 μM DIDS (4,4′-diisothiocyanatostilbene-2,2′-disulphonic acid) greatly enhanced the divalent cation-induced current (10 mM $MgSO_4$). I_{SC}, short circuit current. I_h, holding current necessary to clamp the transepithelial potential to 0 mV in the presence of an ion gradient across the cell layer.

current, if nitrate was present on the basolateral side, but inhibited the current if it was present on the apical side. This indicates that the divalent cation-induced current is due to the movement of Cl^- from the basolateral side to the apical side, but that in the presence of nitrate, nitrate is preferred over Cl^- (Fig. 5*B*).

The divalent cation-induced current was completely blocked by low concentrations of the Cl^- channel blockers flufenamic acid (0.2 μM) and DPC (diphenylamine-2-carboxylatem, 50 μM) (Fig. 5*C*).

As reported above, the CFTR and K^+ channel blocker glibenclamide (0.2 mM) also inhibited the divalent cation-induced current, but it was more effective when applied to the basolateral side, so that this effect is likely to be due to an inhibition of basolateral K^+ channels, rather than CFTR channels (Fig. 5*D*).

The blocker of Cl^- channels and HCO_3^-/Cl^- exchangers, 4,4′-diisothiocyanatostilbene-2,2′-disulphonic acid (DIDS), had no effect on the divalent cation-induced current when applied to the apical side, but greatly enhanced the current when applied to the basolateral side (Fig. 5*E*). This effect was observed both in the presence and the nominal absence of HCO_3^-.

Effects of increased intracellular Ca^{2+} concentrations

$[Ca^{2+}]_i$ was manipulated by the application of the Ca^{2+} ionophores ionomycin and A23187, respectively or by the Ca^{2+} releasing drug thapsigargin. In all cases a current was elicited which greatly exceeded the divalent cation-induced current. Similar to the divalent cation-induced current, the current was enhanced in claudin-16-expressing cells, compared to control cells (Fig. 6*A*) or cells transfected with the claudin-16 mutant R146T. In contrast, responses of cells transfected with the claudin-16 mutant T233R showed currents of almost the same amplitude as those observed in wt claudin-16-transfected cells. The ionomycin-induced current was again clearly sensitive to 50 μM DPC (Fig. 6*B*).

Depletion of the intracellular Ca^{2+} stores with thapsigargin almost completely suppressed any subsequent response of the cell layers to divalent cations, indicating that the release of Ca^{2+} from intracellular stores is responsible for triggering the divalent cation-induced current (Fig. 6*C*).

Effect of divalent cations on the intracellular Ca^{2+} concentration

Differences in response of claudin-16-transfected and control cells to ionomycin and thapsigargin rule out direct interactions between CaSR and claudin-16. The effects, however, might still be due to claudin-16 interacting with the loading of Ca^{2+} stores or with the Cl^- channel.

We therefore measured the effect of an application of 0.1 mM $NiCl_2$ on $[Ca^{2+}]_i$, using the fluorescent indicator fura-2. Under these conditions an increase in $[Ca^{2+}]_i$ was observed as would be expected for CaSR activation. There was no significant difference between $[Ca^{2+}]_i$, increases between wt claudin-16-transfected, R146T mutant claudin-16-transfected, and control cells (Fig. 6*D*).

Furthermore, Ni^{2+} is known to quench fura-2 fluorescence, but no quenching was observed during micro-fluorimetric experiments, when exposing the cells to 100 μM Ni^{2+}. As fura-2 fluorescence quenching allows detection of nanomolar Ni^{2+} concentrations (McCall & Fierke, 2000), an uptake of Ni^{2+} can also be ruled out.

Crosstalk mechanism between claudin-16 and the Ca^{2+}-activated Cl^- channel bestrophin

Recent findings suggest various bestrophin isoforms as candidates for Ca^{2+}-activated Cl^- channels (Qu *et al.* 2004; Tsunenari *et al.* 2006). The presence of bestrophin mRNA in MDCK cells and, as control, in commercial dog kidney cDNA, was therefore further investigated. Two bestrophin isoforms, Best1 and Best4 could be detected and were verified by sequencing. Real-time PCR using commercial probes for dog Best1, Best4 and CaSR revealed the presence of all three RNAs (see Supplementary Fig. S4). There was no difference in mRNA abundance between mock-transfected control cells and wt claudin-16-transfected cells.

We therefore carried out immunohistochemical staining for bestrophin using the antibodies ab14927 (Abcam). As shown in Fig. 7, mock-transfected control cells and claudin-16-transfected cells differed in bestrophin distribution. In claudin-16-transfected cells, the staining pattern indicated bestrophin accumulation in the tight junction region while bestrophin was not localised at cell–cell contacts in control cells. Staining of R146T mutant-transfected cells showed a bestrophin distribution similar to control cells (Fig. 8*A* and *B*). In contrast, T233R mutant-transfected cells showed the same staining pattern as wt claudin-16 (Fig. 8*C*–*E*). Thus, accumulation of bestrophin was only found in cells exhibiting enhanced Cl^- secretion when stimulated with divalent cations.

Based on these data, we propose that increased Cl^- secretion in claudin-16-expressing cells may be due to direct or indirect interaction between claudin-16 and the apical Ca^{2+}-activated Cl^- channel bestrophin.

Discussion

Paracellular ion transport depends on tight junction permeability as well as on transcellular driving forces.

As a general result, we found that both were altered by claudin-16 and that this may explain the full effect of defective forms of claudin-16 on Mg^{2+} and Ca^{2+} transport.

Claudin-16 and paracellular ion permeability

Changes in paracellular permeabilities have been studied in different claudin-16-transfected cell models with conflicting results. Hou *et al.* (2005) found that claudin-16 increased the Na^+ permeability (P_{Na}) in layers of transfected LLC-PK1 cells, without affecting Cl^- permeability (P_{Cl}). Effects on Mg^{2+} permeability (P_{Mg}) in these cells were significant but small. Both effects were augmented in the presence of claudin-19 which additionally decreased P_{Cl} (Hou *et al.* 2008). In contrast to these findings in LLC-PK1 cells, Hou *et al.* (2005) found no significant effects of claudin-16 on P_{Na}, P_{Cl} or P_{Mg} in low resistance MDCK-II cells.

Ikari *et al.* (2004, 2006) also used low resistance MDCK cells and found a decrease in P_{Na} when expressing claudin-16, but an increase in Ca^{2+} and Mg^{2+} flux (apical to basolateral), while Ca^{2+} flux in the opposite direction remained unchanged.

In our previous (Kausalya *et al.* 2006) as well as in the present study, we transfected high resistance MDCK-C7 cells with claudin-16 and found an increased P_{Mg}, but no effects on P_{Na}, P_{Cl} or P_{Ca}. Mg^{2+} and Ca^{2+} fluxes occurred similarly in both directions.

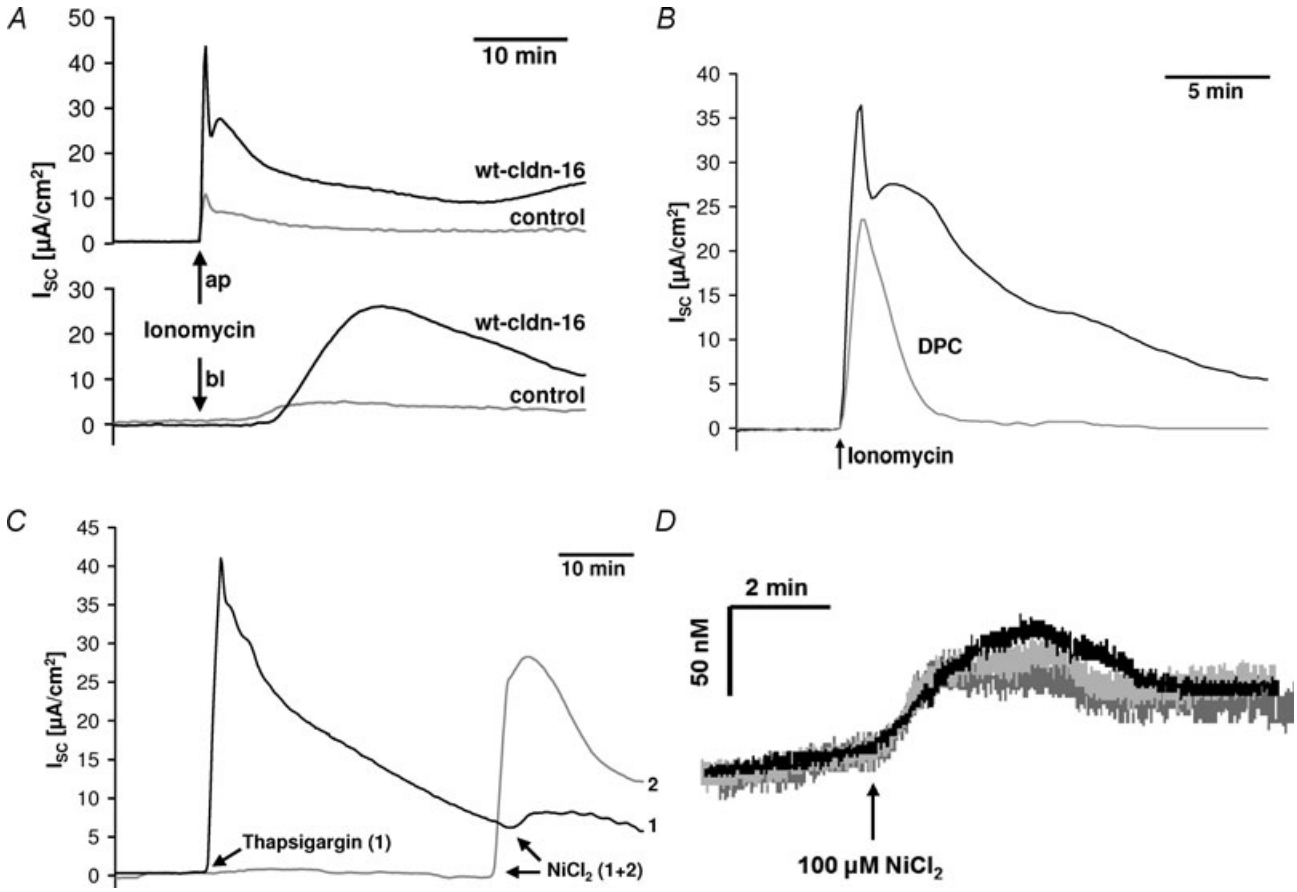

Figure 6. Involvement of intracellular Ca^{2+}
A–C, black traces, wt claudin-16-transfected cells; grey traces, mock-transfected cells. *A*, application of 10^{-8} M ionomycin induced a current which was considerably larger in wt claudin-16-transfected cells than in mock-transfected controls. Application of ionomycin to the apical side caused an instantaneous, rapid increase in current while application to the basolateral side slowed the current increase and delayed it by several minutes. *B*, the current induced by ionomycin (10^{-8} M) was sensitive to low concentrations (50 μM) of DPC (diphenylamine-2-carboxylate). *C*, thapsigargin (10^{-6} M)-induced release of Ca^{2+} from intracellular stores caused an instantaneous rise in current. Subsequent application of 100 μM $NiCl_2$ induced only a minor increase in current compared to the current elicited in cell layers not pretreated with thapsigargin. *D*, divalent cation-induced increases in $[Ca^{2+}]_i$ measured with fura-2 did not differ between wt claudin-16-transfected (black trace), R146T mutant-transfected (light grey trace) or mock-transfected control cells (dark grey trace). I_{SC}, short circuit current.

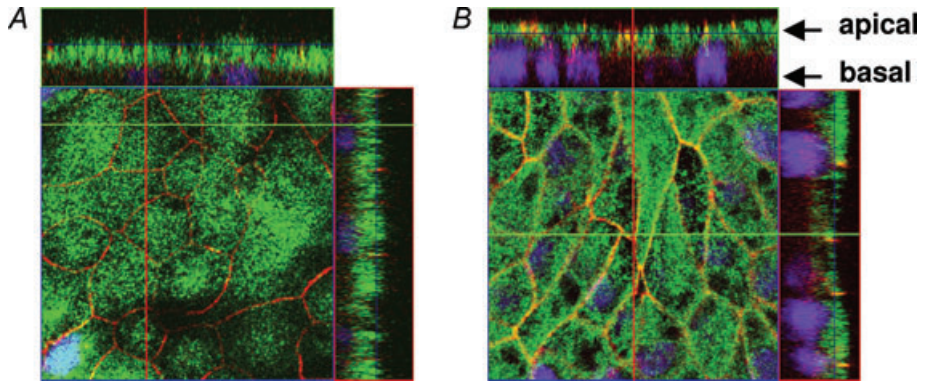

Figure 7. Localization of bestrophin in mock-transfected and claudin-16-transfected cells
A, confocal laser-scanning micrographs of mock-transfected, and *B*, wt claudin-16 (short version)-transfected MDCK-C7 cells. Red, occludin; green, bestrophin; blue, nuclei (DAPI). The yellow colour along the cell–cell contacts in *B* indicates co-localization of occludin and bestrophin. This was not found in control cells. Z scans indicate that bestrophin accumulated not only at tight junctions but generally in the apical membrane.

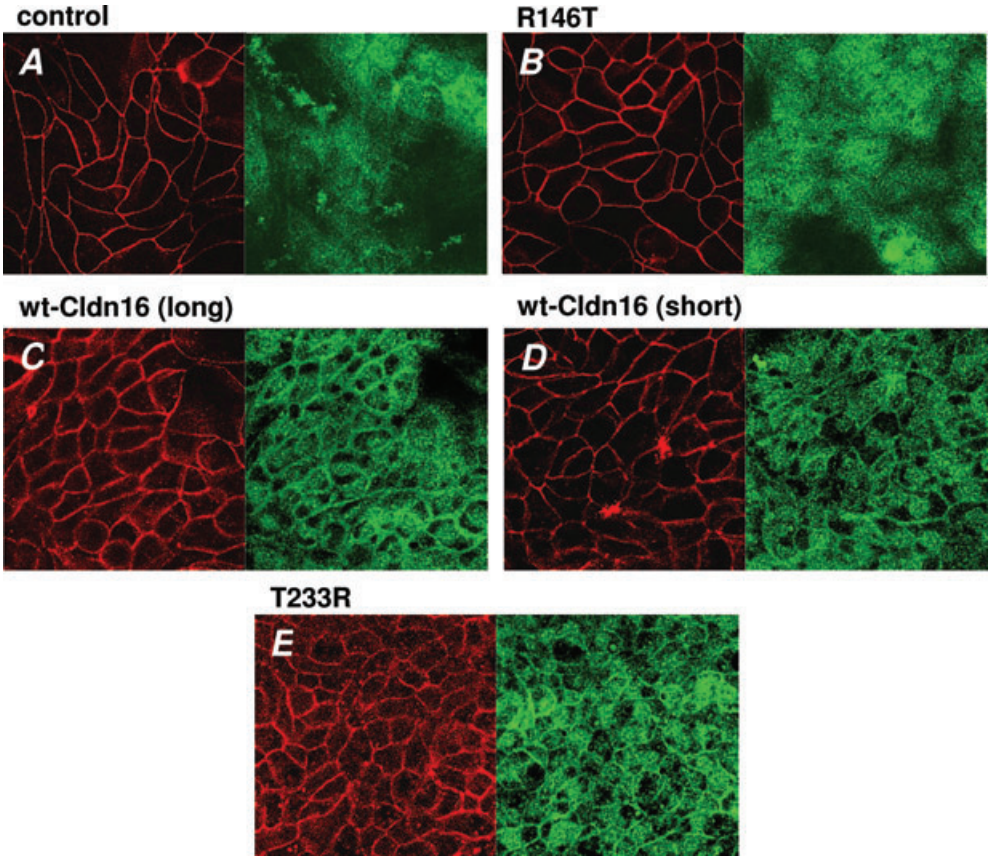

Figure 8. Localization of bestrophin in mutant claudin-16-transfected cells
Confocal laser-scanning micrographs of wt claudin-16-, mutant claudin-16-, and mock-transfected MDCK-C7 cells. Red, occludin; green, bestrophin; blue, nuclei (DAPI). All micrographs were obtained in the plane of the tight junction, as indicated by the clearly visible occludin signal. *A* and *B*, distribution of bestrophin in mock-transfected control cells and R146T mutant-transfected cells was diffuse. *C–E*, cells exhibiting strong divalent cation-induced current (wt claudin-16- and T233R mutant-transfected cells) showed a prominent accumulation of bestrophin in the tight junction region.

Thus, the only consistent effect in the different cell types compared to control cells is the increase, albeit small, in P_{Mg} in wt claudin-16-transfected cells, which is absent in cells transfected with mutant claudin-16. Considering the dramatic effect of defects in claudin-16 on Mg^{2+} homeostasis in FHNNC patients, the effect of claudin-16 on P_{Mg} appears surprisingly small.

The reason for the variability of the effects of claudin-16 expression on all other paracellular parameters observed in the different studies is unclear. A possible reason may be the use of different cell lines (i.e. MDCK-C7 *vs* MDCK-II or LLC-PK1), which differ in their endogenous claudin repertoire that may alter the effects of exogenous claudins (Van Itallie *et al.* 2003). Furthermore, it cannot be ruled out that claudin-16 specifically needs claudin-19 as an interaction partner to fully unfold its function (Hou *et al.* 2008).

In addition, differences in findings relating to P_{Ca} may also be related to methodological differences. Low extracellular Ca^{2+} concentrations, as used by Ikari *et al.* (2004, 2006) for example, are known to open tight junctions. To avoid this problem in the present study, extracellular Ca^{2+} concentrations during Ca^{2+} flux experiments were kept at 1.2 mM on both the apical and the basolateral side of the cell layers.

Transcellular current

The possibility that the Mg^{2+}-induced transcellular current observed in the present study might be caused by reversal of an electrogenic, Na^+-dependent, transcellular Mg^{2+} transport could be ruled out by the finding that a current with identical properties could be induced in the nominal absence of extracellular Mg^{2+} by the application of various other divalent cations. Some of these cations, such as Ni^{2+}, are known to quench fura-2 fluorescence. As no quenching was observed during application of 100 μM Ni^{2+}, Ni^{2+} uptake could also be ruled out.

The features of the divalent cation-induced current are consistent with those published for CaSR and cation-sensing receptor (CSR) activation (CaSR, Arthur *et al.* 1997; Faurskov & Bjerregaard, 2002; CSR, Chang & Shoback, 2004; Ward, 2004): CaSR can be activated through extracellular divalent and trivalent cations. For Mg^{2+} stimulation, an EC_{50} of 4.5 mM (Ruat *et al.* 1996) and 4.7 mM (Bräuner-Osborne *et al.* 1999) and a Hill coefficient of 2.3 (Bräuner-Osborne *et al.* 1999) have been reported, values that are strikingly similar to those found in the present study (see Fig. 3*A*). EC_{50} values are surprisingly high; however, there are estimates that interstitial concentrations in this order of magnitude may be reached at least in the medulla of the kidney (Brunette *et al.* 1978).

CaSR is coupled to a G-protein and is known to act through a cAMP decrease and through IP_3-induced Ca^{2+} release from intracellular stores (Arthur *et al.* 1997; Ward, 2004). Furthermore, in MDCK cells an increase in $[Ca^{2+}]_i$ triggers Cl^- secretion (Lahr *et al.* 2000).

In a recent study, Ikari *et al.* (2008) postulate an interaction between CaSR and claudin-16-mediated Mg^{2+} transport via PKA inhibition, decreased claudin-16 phosphorylation and a resulting claudin-16 translocation to lysosomes.

Our present model for the divalent cation-induced transcellular current in claudin-16-transfected MDCK-C7 cells is depicted in Fig. 9 and differs fundamentally from the model suggested by Ikari *et al.* (2008). In part the present model is comparable with a model published by Lahr *et al.* (2000) for antidiuretic hormone (ADH) stimulation of MDCK cells, where activation of V1 receptors causes Ca^{2+} release from intracellular stores and the activation of apical Ca^{2+}-sensitive Cl^- channels.

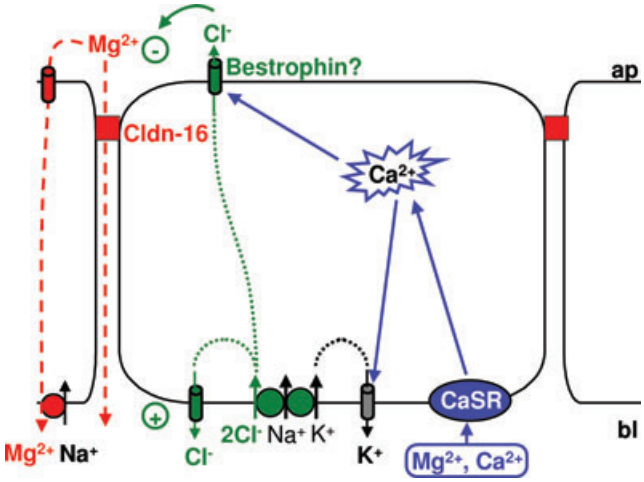

Figure 9. Model of components involved in the generation of the divalent cation-induced Cl^- current in claudin-16-transfected MDCK-C7 cells
Application of divalent cations to the basolateral side of claudin-16-expressing MDCK-C7 cell layers activates the Ca^{2+}-sensing receptor, CaSR. This causes release of Ca^{2+} from intracellular stores and thus an increase in $[Ca^{2+}]_i$. Intracellular Ca^{2+} activates the apical Ca^{2+}-sensitive Cl^- channel bestrophin, which, in claudin-16-expressing cells, is recruited to the apical membrane and to the tight junction, i.e. close to the release sites of Ca^{2+} from intracellular stores. Cl^- enters the cells through basolateral Na^+-dependent, K^+-dependent or independent symport mechanisms and, under resting conditions, probably leaves the cells through basolateral, DIDS-sensitive Cl^- channels. When, upon CaSR stimulation, apical Cl^- channels open, Cl^- is able to leave the cells on the apical side, thus carrying the observed current. K^+ entering the cells together with Cl^- on the basolateral side can leave the cells on the basolateral side through Ca^{2+}-sensitive K^+ channels. This helps to further enhance the observed divalent cation-induced current. This current changes the transepithelial potential and thus the driving force for both para- and transcellular transport of Mg^{2+} (and Ca^{2+}).

In the present model, application of divalent cations to the basolateral side of the cell layer causes CaSR activation, which triggers an increase in $[Ca^{2+}]_i$, thereby activating a transcellular current (Cl^- secretion, see below). The $[Ca^{2+}]_i$ increase appears to be predominantly due to Ca^{2+} release from intracellular stores, as store depletion by thapsigargin prevents consecutive activation of the current by application of divalent cations. Conversely, the transcellular current can be activated by direct manipulations of $[Ca^{2+}]_i$, e.g. by the application of Ca^{2+} ionophores (ionomycin, A23187) or during the depletion of Ca^{2+} stores through the application of thapsigargin and/or caffein.

The increase in $[Ca^{2+}]_i$ causes activation of apical Ca^{2+}-sensitive Cl^- channels and basolateral Ca^{2+}-sensitive K^+ channels and thus induces Cl^- secretion, which is energized by a basolateral furosemide/bumetanide-sensitive Na^+-K^+-$2Cl^-$ symport and a basolateral chlorothiazide-sensitive Na^+-Cl^- symport. Therefore, a respective removal of basolateral Na^+ and Cl^- (replaced with non-permeant anions) completely inhibits the transcellular current, while removal of basolateral K^+ only causes partial inhibition. K^+ has to leave the cells through the basolateral Ca^{2+}-sensitive K^+ channels, as an inhibition of these channels reduces the observed current. Cl^- partially leaks out at the basolateral side through DIDS-sensitive channels or transporters. Hence, basolateral application of DIDS increases the current.

So, how does claudin-16 modulate the pathway leading to Cl^- secretion? One possibility is that claudin-16 interacts with CaSR. Alternatively, claudin-16 could affect the loading of intracellular Ca^{2+} stores, or interact with the apical, Ca^{2+}-sensitive Cl^- channels.

An interaction between claudin-16 and CaSR is unlikely based on the observation that intracellular Ca^{2+} increases induced by thapsigargin and ionomycin are able to mimick the divalent cation-induced currents. Furthermore, a claudin-16 interaction with the loading of intracellular Ca^{2+} stores is also unlikely. First, $[Ca^{2+}]_i$ transients observed after CaSR activation did not differ between claudin-16- and mock-transfected control cells (Fig. 6*D*). Second, ionomycin effects differ between wt claudin-16-transfected, mutant claudin-16-transfected and control cells. As ionomycin-induced $[Ca^{2+}]_i$ increases should be store independent, this indicates that components down-stream of the $[Ca^{2+}]_i$ increases are responsible for the observed differences.

Bestrophin

An interaction between claudin-16 and apical Ca^{2+}-activated Cl^- channels therefore seems most likely. Unfortunately, the molecular identity of Ca^{2+}-activated Cl^- channels is still controversial (Qu *et al.* 2003). While members of the CLCA (chloride channel, calcium-activated) family are either not blocked by niflumic acid or only at near-millimolar concentrations, the Cl^- current observed in the present study was completely blocked by micromolar concentrations of the structurally similar flufenamic acid. Another Ca^{2+}-activated Cl^- channel candidate is bestrophin, which is predominantly expressed in the retinal pigment epithelium and has been linked to Best disease (Petrukhin *et al.* 1998). However, bestrophin expression has been reported for other tissues such as liver, spleen, colon and, interestingly, kidney (Qu *et al.* 2003; Barro Soria *et al.* 2006). In this context, it is noteworthy that about one third to one half of the FHNNC patients present ocular abnormalities (Meij *et al.* 2002). In contrast to the CLCA Cl^- channels, bestrophin is inhibited by niflumic acid at concentrations as low as 10 μM (Pifferi *et al.* 2006).

Interestingly, we observed that the subcellular distribution of bestrophin differed in wt claudin-16 and T233R mutant claudin-16-transfected cells compared to R146T mutant claudin-16 or control cells. Bestrophin showed a diffuse distribution in control cells, similar to the recently reported localization of bestrophin-1 in the endoplasmic reticulum of HEK293 cells (Aldehni *et al.* 2009). Howewer, bestrophin was concentrated near the apical membrane and at the site of cell–cell contacts in claudin-16-overexpressing cells, where it partially colocalized with occludin. This relocalization correlated with the presence of strong divalent cation-induced currents as induced by wt claudin-16 or the T233R mutant. Incidentally, release of Ca^{2+} from the endoplasmic reticulum has been reported to occur from this region in polarized MDCK cells (Colosetti *et al.* 2003). Claudin-16 may thus optimise the localization of Ca^{2+}-activated Cl^- channels to areas of high $[Ca^{2+}]_i$ during the release of Ca^{2+} from intracellular stores. Bestrophin is thus an attractive candidate for mediating the claudin-16-dependent transcellular current observed in MDCK cells and further research will test this hypothesis.

Wt-claudin-16 and claudin-16 mutants

We did not detect a functional diversity between 'human' and 'rodent' claudin-16: MDCK cells expressing either the long or the short version of claudin-16 showed identical properties with regard to paracellular Mg^{2+} and Ca^{2+} flux and to the increase in divalent cation-induced Cl^- current.

The two mutants investigated showed contrasting behaviour. The R146T mutant, which affects net charge of the second extracellular loop, still resides within the tight junction (Kausalya *et al.* 2006), but transfected cells show neither increased paracellular fluxes nor increased transcellular currents and thus lack both components of wt claudin-16. In affected patients, this mutation causes FHHNC (Weber *et al.* 2001*b*). The T233R mutant affects the PDZ binding motif of claudin-16 and thus correct

localization within the tight junction (Kausalya *et al.* 2006). Cells expressing this mutant do not show increased paracellular Mg^{2+} flux but still exhibit the increased transcellular current. Patients carrying this mutation only show a mild form of FHHNC (Müller *et al.* 2003).

It is thus concluded that the increased paracellular flux requires an intact claudin-16 and a correct localization within the tight junction. Both the long and the short claudin-16 version serve equally well.

Together with the observation that cells overexpressing another claudin, namely claudin-11, do not exhibit the increased divalent cation-induced Cl^- current, it can be concluded that this current is not a mere artefact of the overexpression of a tight junction protein. The observation that the T233R mutant does not reside within the tight junction but retains the increased divalent cation-induced Cl^- current argues against a direct interaction between bestrophin and claudin-16 or at least against an interaction via the PDZ-binding motif. The molecular details of this interaction will be investigated in a future study.

Physiological implications

TAL cells and MDCK cells are both equipped with Na^+-K^+-$2Cl^-$ symporters and Cl^- channels, but these transporters are arranged in a mirror-like orientation in both cell types. Therefore, net Cl^- transport is directed from the basolateral to the apical side in MDCK cell layers but in the reverse direction in TAL cells.

Nevertheless, due to the lack of TAL cell lines that can be grown to form confluent monolayers, claudin-16-transfected MDCK cells represent the best model system currently available to explore the functional roles of claudin-16.

It might be tempting to extrapolate the findings obtained in MDCK cells to TAL cells since, similar to MDCK cells, these cells also possess a basolateral CaSR (Chattopadhyay *et al.* 1996; Desfleurs *et al.* 1998). Although stimulation of CaSR in the TAL is known to dissipate the transepithelial potential and thus the driving force for Mg^{2+} absorption, the underlying mechanisms are different from those observed in MDCK cells.

Thus, the situation in MDCK cells may better reflect that of more distal parts of the nephron, where claudin-16 is also expressed (Simon *et al.* 1999). In this region of the nephron, fine-tuning of renal Mg^{2+} homeostasis takes place and claudin-16 may crosstalk with the CaSR to control Mg^{2+} transport.

References

Aldehni F, Barro Soria R, Almaca J, Raquel Martins J, Ousingsawat J, Schreiber R & Kunzelmann K (2009). ER localized and Pak2 phosphorylated bestrophin 1 confers receptor activation of epithelial Ca^{2+} dependent ion channels. *Acta Physiol* **195** (Suppl 669), P472.

Amasheh S, Meiri N, Gitter AH, Schöneberg T, Mankertz J, Schulzke JD & Fromm M (2002). Claudin-2 expression induces cation-selective channels in tight junctions of epithelial cells. *J Cell Sci* **115**, 4969–4976.

Arthur JM, Collinsworth GP, Gettys TW, Quarles LD & Raymond JR (1997). Specific coupling of a cation-sensing receptor to G protein a-subunits in MDCK cells. *Am J Physiol Renal Physiol* **273**, F129–F135.

Barro Soria R, Spitzner M, Schreiber R & Kunzelmann K (2006). Bestrophin 1 enables Ca^{2+} activated Cl^- conductance in epithelia. *J Biol Chem*; DOI: 10.1074/jbc.M605716200.

Bräuner-Osborne H, Jensen AA, Sheppard PO, O'Hara P & Krogsgaard-Larsen P (1999). The agonist-binding domain of the calcium-sensing receptor is located at the amino-terminal domain. *J Biol Chem* **274**, 18382–18386.

Brunette MG, Vigneault N & Carriere S (1978). Magnesium handling by the papilla of the young rat. *Pflügers Arch* **373**, 229–235.

Chang W & Shoback D (2004). Extracellular Ca^{2+}-sensing receptors – an overview. *Cell Calcium* **35**, 183–196.

Chattopadhyay N, Baumm M, Bai M, Riccardi D, Hebert SC, Harris HW & Brown EM (1996). Ontogeny of the extracellular calcium-sensing receptor in rat kidney. *Am J Physiol Renal Physiol* **271**, F736–F743.

Cole DEC & Quamme GA (2000). Inherited disorders of renal magnesium handling. *J Am Soc Nephrol* **11**, 1937–1947.

Colosetti P, Tunwell REA, Cruttwell C, Jean-Pierre Arsanto J-P, Mauger JP & Cassio D (2003). The type 3 inositol 1,4,5-trisphosphate receptor is concentrated at the tight junction level in polarized MDCK cells. *J Cell Sci* **116**, 2791–2803.

Desfleurs E, Wittner M, Simeone S, Pajaud S, Moine G, Rajerison R & Di Stefano A (1998). Calcium-sensing receptor: regulation of electrolyte transport in the thick ascending limb of Henle's loop. *Kidney Blood Press Res* **21**, 401–412.

Di Stefano A, Roinel N, de Rouffignac C & Wittner M (1993). Transepithelial Ca^{2+} and Mg^{2+} transport in the cortical thick ascending limb of Henle's loop of the mouse is a voltage-dependent process. *Ren Physiol Biochem* **16**, 157–166.

Faurskov B & Bjerregaard HF (2002). Evidence for cadmium mobilization of intracellular calcium through a divalent cation receptor in renal distal epithelial A6 cells. *Pflügers Arch* **445**, 40–50.

Gekle M, Wünsch S, Oberleithner H & Silbernagl S (1994). Characterization of two MDCK-cell subtypes as a model system to study principal cell and intercalated cell properties. *Pflügers Arch* **428**, 157–162.

Grynkiewicz G, Poenie M & Tsien RY (1985). A new generation of Ca^{2+} indicators with greatly improved fluorescence properties. *J Biol Chem* **260**, 3440–3450.

Günzel D, Haisch L, Pfaffenbach S, Krug SM, Milatz S, Amasheh S, Hunziker W & Müller D (2009*a*). Claudin function in the thick ascending limb of Henle's loop. *Ann NY Acad Sci* **1165**, 1507–1517.

Günzel D, Stuiver M, Kausalya PJ, Haisch L, Krug SM, Rosenthal R, Meij IC, Hunziker W, Fromm M & Müller D (2009*b*). Claudin-10 exists in six alternatively spliced isoforms which exhibit distinct localization and function. *J Cell Sci* **122**, 1507–1517.

Hirano T, Kobayashi N, Itoh T, Takasuga A, Nakamaru T, Hirotsune S & Sugimoto Y (2000). Null mutation of PCLN-1/claudin-16 results in bovine chronic interstitial nephritis. *Genome Res* **10**, 659–663.

Hochstrate P, Piel C & Schlue WR (1995). Effect of extracellular K^+ on the intracellular free Ca^{2+} concentration in leech glial cells and Retzius neurones. *Brain Res* **696**, 231–241.

Hou J, Paul DL & Goodenough DA (2005). Paracellin-1 and the modulation of ion selectivity of tight junctions. *J Cell Sci* **118**, 5109–5118.

Hou J, Renigunta A, Konrad M, Gomes AS, Schneeberger EE, Paul DL, Waldegger S & Goodenough DA (2008). Claudin-16 and claudin-19 interact and form a cation-selective tight junction complex. *J Clin Invest* **118**, 619–628.

Ikari A, Hirai N, Shiroma M, Harada H, Sakai H, Hayashi H, Suzuki Y, Degawa M & Takagi K (2004). Association of paracellin-1 with ZO-1 augments the reabsorption of divalent cations in renal epithelial cells. *J Biol Chem* **279**, 54826–54832.

Ikari A, Matsumoto S, Harada H, Takagi K, Hayashi H, Yuichi Suzuki Y, Degawa M & Miwa M (2006). Phosphorylation of paracellin-1 at Ser217 by protein kinase A is essential for localization in tight junctions. *J Cell Sci* **119**, 1781–1789.

Ikari A, Okude C, Sawada H, Sasaki Y, Yamazaki Y, Sugatani J, Degawa M & Miwa M (2008). Activation of a polyvalent cation-sensing receptor decreases magnesium transport via claudin-16. *Biochim Biophys Acta* **1778**, 283–290.

Itoh M, Furuse M, Morita K, Kubota K, Saitou M & Tsukita S (1999). Direct binding of three tight junction-associated MAGUKs, ZO-1, ZO-2, and ZO-3, with the COOH termini of claudins. *J Cell Biol* **147**, 1351–1363.

Kausalya PJ, Amasheh S, Günzel D, Wurps H, Müller D, Fromm M & Hunziker W (2006). Disease-associated mutations affect intracellular traffic and paracellular Mg^{2+} transport function of claudin-16. *J Clin Invest* **116**, 878–891.

Kiuchi-Saishin Y, Gotoh S, Furuse M, Takasuga A, Tano Y & Tsukita S (2002). Differential expression patterns of claudins, tight junction membrane proteins, in mouse nephron segments. *J Am Soc Nephrol* **13**, 875–886.

Kreusel KM, Fromm M, Schulzke JD & Hegel U (1991). Cl^- secretion in epithelial monolayers of mucus-forming human colon cells (HT-29/B6). *Am J Physiol Cell Physiol* **261**, C574–C582.

Lahr TF, Record RD, Hoover DK, Hughes CL & Blazer-Yost BL (2000). Characterization of the ion transport responses to ADH in the MDCK-C7 cell line. *Pflügers Arch* **439**, 610–617.

McCall KA & Fierke CA (2000). Colorimetric and fluorimetric assays to quantitate micromolar concentrations of transition metals. *Anal Biochem* **284**, 307–315.

Meij IC, Van Den Heuvel LP & Knoers NV (2002). Genetic disorders of magnesium homeostasis. *BioMetals* **15**, 297–307.

Müller D, Kausalya PJ, Bockenhauer D, Thumfart J, Meij IC, Dillon MJ, van't Hoff W & Hunziker W (2006*a*). Unusual clinical presentation and possible rescue of a novel claudin-16 mutation. *J Clin Endocrinol Metab* **91**, 3076–30769.

Müller D, Kausalya PJ, Claverie-Martin F, Meij IC, Eggert P, Garcia-Nieto V & Hunziker W (2003). A novel claudin-16 mutation associated with childhood hypercalciuria abolishes binding to ZO-1 and results in lysosomal mistargeting. *Am J Hum Genet* **73**, 1293–1301.

Müller D, Kausalya PJ, Meij IC & Hunziker W (2006*b*). Familial hypomagnesemia with hypercalciuria and nephrocalcinosis: blocking endocytosis restores surface expression of a novel claudin-16 mutant that lacks the entire C-terminal cytosolic tail. *Hum Mol Genet* **15**, 1049–1058.

Petrukhin K, Koisti MJ, Bakall B, Li W, Xie G, Marknell T *et al.* (1998). Identification of the gene responsible for Best macular dystrophy. *Nat Genet* **19**, 241–247.

Pifferi S, Pascarella G, Boccaccio A, Mazzatenta A, Gustincich S, Menini A & Zucchelli S (2006). Bestrophin-2 is a candidate calcium-activated chloride channel involved in olfactory transduction. *Proc Natl Acad Sci U S A* **103**, 12929–12934.

Praga M, Vara J, Gonzalez-Parra E, Andres A, Alamo C, Araque A, Ortiz A & Rodicio JL (1995). Familial hypomagnesemia with hypercalciuria and nephrocalcinosis. *Kidney Int* **47**, 1419–1425.

Qu Z, Fischmeister R & Hartzell C (2004). Mouse bestrophin-2 is a bona fide Cl^- channel: identification of a residue important in anion binding and conduction. *J Gen Physiol* **123**, 327–340.

Qu Z, Wei RW & Hartzell HC (2003). Characterization of Ca^{2+}-activated Cl^- currents in mouse kidney inner medullary collecting duct cells. *Am J Physiol Renal Physiol* **285**, F326–F335.

Ruat M, Snowman AM, Hester LD & Snyder SH (1996). Cloned and expressed rat Ca^{2+}-sensing receptor. Differential cooperative responses to calcium and magnesium. *J Biol Chem* **271**, 5972–5975.

Schlingmann KP & Gudermann T (2005). A critical role of TRPM channel-kinase for human magnesium transport. *J Physiol* **566**, 301–308.

Simon DB, Lu Y, Choate KA, Velazquez H, Al-Sabban E, Praga M *et al.* (1999). Paracellin-1, a renal tight junction protein required for paracellular Mg^{2+} resorption. *Science* **285**, 103–106.

Tsunenari T, Nathans J & Yau KW (2006). Ca^{2+}-activated Cl^- current from human bestrophin-4 in excised membrane patches. *J Gen Physiol* **127**, 749–754.

Van Itallie CM, Fanning AS & Anderson JM (2003). Reversal of charge selectivity in cation or anion-selective epithelial lines by expression of different claudins. *Am J Physiol Renal Physiol* **285**, F1078–F1084.

Ward DT (2004). Calcium receptor-mediated intracellular signalling. *Cell Calcium* **35**, 217–228.

Weber S, Hoffmann K, Jeck N, Saar K, Boeswald M, Kuwertz-Broeking E *et al.* (2000). Familial hypomagnesaemia with hypercalciuria and nephrocalcinosis maps to chromosome 3q27 and is associated with mutations in the PCLN-1 gene. *Eur J Hum Genet* **8**, 414–422.

Weber S, Schlingmann KP, Peters M, Nejsum LN, Nielsen S, Engel H *et al.* (2001*a*). Primary gene structure and expression studies of rodent paracellin-1. *J Am Soc Nephrol* **12**, 2664–2672.

Weber S, Schneider L, Peters M, Misselwitz J, Ronnefarth G, Boswald M *et al.* (2001*b*). Novel paracellin-1 mutations in 25 families with familial hypomagnesemia with hypercalciuria and nephrocalcinosis. *J Am Soc Nephrol* **12**, 1872–1881.

Author contributions

D.G., M.F.: conception and design of data. D.G., S.A., S.P., P.J.K.: performing experiments. D.G.: drafting the article. All authors: analysis and interpretation of data, revising the article critically for important intellectual content, and final approval of the version to be published.

Acknowledgements

We gratefully acknowledge the skilful technical assistance of Sieglinde Lüderitz, Brigitte Papanis and Detlef Sorgenfrei. Supported by the Deutsche Forschungsgemeinschaft (DFG GU447/11-1 and DFG Research Unit FOR 721).